Lattice dynamics and the interaction with the crystal electric field in $NdCu_2$



2004 J. Phys.: Condens. Matter 16 5751

(http://iopscience.iop.org/0953-8984/16/32/012)

INSTITUTE OF PHYSICS PUBLISHING JOURNAL OF PHYSICS: CONDENSED MATTER

J. Phys.: Condens. Matter **16** (2004) 5751–5768 PII: S0953-8984(04)82238-0

# Lattice dynamics and the interaction with the crystal electric field in $NdCu_2$

**K Hense[1], E Gratz[1], H Nowotny[2] and A Hoser[3]**

[1] Institute for Solid State Physics, Vienna University of Technology, Wiedner Hauptstraße 8-10, 1040 Wien, Austria
[2] Institute for Theoretical Physics, Vienna University of Technology, Wiedner Hauptstraße 8-10, 1040 Wien, Austria
[3] IFF, Forschungszentrum, Jülich, Germany

E-mail: gratz@ifp.tuwien.ac.at

Received 17 June 2004
Published 30 July 2004
Online at stacks.iop.org/JPhysCM/16/5751
doi:10.1088/0953-8984/16/32/012

**Abstract**

The lattice dynamics of $NdCu_2$ has been investigated with inelastic neutron scattering measurements. An uniaxial Born–von Karman model has been used to calculate the phonon dispersion relation. A verification of a phonon–crystal electric field (CEF) interaction was found from temperature dependent measurements of phonons and CEF excitations. The impact of the phonon–CEF interaction was found to be strongest at the Brillouin zone centre among the 7.5 meV $A_g$-phonon mode and the $\varepsilon_4$ CEF level. This has been verified with theoretical model calculations.

## 1. Introduction

Crystal electric field (CEF) phenomena are single particle excitations, well known to exist in rare earth based compounds. The ground state multiplet of a RE-ion with total momentum $J$ is split into a series of CEF states due to the electric field caused by the surrounding ions in a solid. In contrast, phonons are collective phenomena where more than $10^{10}$ particles are participating. An interaction of both phenomena (lattice vibrations and CEF excitations) are based on the following idea. The lattice vibrations causes a change of the local electric field in the neighbourhood of a given RE-ion and thus a change of the CEF excitation energies. However, normally this kind of interaction among both phenomena is too small to be observed in experiment (neutron diffraction, Raman spectroscopy, etc), although there are a few cases known where an interaction of the phonons and the CEF has been verified. One of the first reports about such an interaction concerns the cubic Laves phases $CeAl_2$. In this compound a softening of the acoustic phonon branches with decreasing temperature was explained as being caused by the CEF–phonon interaction [1]. A theoretical description of this phenomena was given by Thalmeier and Fulde [2, 3]. Later a CEF–phonon interaction was observed in the

  

Raman spectra of $LiTbF_4$ by Dörfer and Schraak [4]. More recently evidence for this kind of interaction has been verified in $NdBa_2Cu_3O_{7-\delta}$ [5–7] and $Pr_2Sr_2NdBa_2Cu_3O_{8+\delta}$ [8]. The first hints for the existence of the CEF–phonon interaction within the family of $RCu_2$ compounds were reported for $CeCu_2$ by Loewenhaupt [9, 10]. Detailed investigations of the CEF–phonon interaction in $CeCu_2$ based on neutron diffraction experiments are in progress and will be published soon. $NdCu_2$ crystallizes like $CeCu_2$ in an orthorhombic structure with the space group *Imma*. This compound orders antiferromagnetically at 6.5 K [11]. Among the family of $RCu_2$ compounds $NdCu_2$ is by far the most intensively investigated [11–18].

After we finished the study of the lattice dynamics of the isostructural nonmagnetic $YCu_2$ compound [19] we continued to investigate also the lattice dynamics of the $RCu_2$ compounds beginning with $NdCu_2$. We expected that if a CEF–phonon interaction in $NdCu_2$ is detectable in neutron experiments, it should be observable when studying the temperature variation of either the lattice dynamics or the CEF excitations. Thus the aim of this study was twofold: to measure the lattice dynamics of $NdCu_2$ and to verify the existence of the CEF–phonon interaction.

## 2. Experimental details

### *2.1. Tripple axis spectrometer measurements*

The single crystal used for the experiments is called in the literature the 'Viennese Crystal' [14, 16, 17, 20]. With this crystal, triple axis spectrometer measurements were carried out with the UNIDAS spectrometer (FZ-Jülich), the E1 spectrometer (HMI-Berlin), and with the 1T1 spectrometer (LLB-Saclay). UNIDAS and E1 measurements were carried out in the constant-$k_i$ mode, whereas the 1T1 spectrometer was used in the constant-$k_f$ mode. In all the experiments the (002) Bragg-reflection of pyrolytic graphite was used as monochromator and analyser. In order to prevent contamination of higher order harmonics, a PG-filter was inserted in the incoming beam (E1 and UNIDAS), or in the outgoing beam (1T1). For the 1T1 a bend analyser and monochromator was used, whereas for the UNIDAS and the E1 spectrometer {open-40′-40′-open} or {open-40′-40′-40′} collimation was used. All spectrometers have been used in the 'zig-zag' configuration.

### *2.2. Time of flight measurements*

Time of flight measurement on a powdered sample material of $NdCu_2$ were performed on the LRMECS spectrometer at Argonne. The incoming neutron energy in the LRMECS experiment was 35 meV. The energy resolution was about 2 meV.[4] Below 4 meV, the elastic and quasi-elastic contributions can hardly be separated from the data in this experiment, therefore, data of this region has to be excluded from the investigation. The phonon density of states (PDOS) in the region below 4 meV has been approximated by a quadratic increase as a function of energy, as expected from the linear slope of the acoustic phonon branches.

## 3. Phonons in $NdCu_2$

### *3.1. Crystal structure*

Most of the $RCu_2$ compounds crystallize in the orthorhombic $CeCu_2$-type structure. This structure belongs to the nonsymmorphic space group *Imma* ($D_{2h}^{28}$). The R-ions occupy the Wyckoff 4(e) sites ($C_{2v}^{z}$ symmetry) and the Cu-ions the 8(h) sites ($C_s$ symmetry). There exist only two nonequivalent ion positions, one for the R- and one for the Cu-ions. Three position

[4] http://www.pns.anl.gov/lrmecs/lrmecs.html

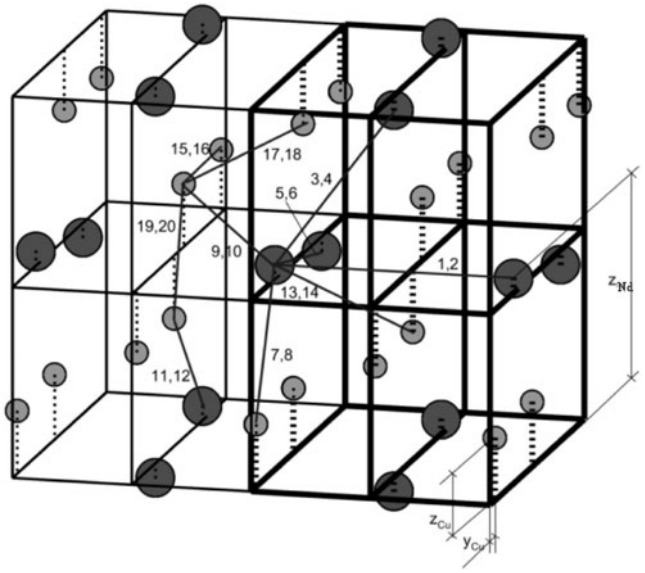


**Figure 1.** Ion arrangement in two adjacent orthorhombic unit cells of $NdCu_2$. The large symbols indicate the Nd-ions and the small symbols the Cu-ions. The lines and the numbers indicate the springs taken into account in the Born–von Karman spring model (see table 2).

**Table 1.** Structure parameters for $NdCu_2$. The space group of this structure is *Imma* (Nr. 74), $a = 4.3917 \pm 0.0004$ Å, $b = 7.0350 \pm 0.0006$ Å, $c = 7.4186 \pm 0.0011$ Å. Nd-ions occupy the 4(e)-sites, Cu-ions the 8(h)-sites. The neodymium fractional position parameter is $z_{Nd} = 0.5383$, these of copper are $y_{Cu} = 0.0506$, $z_{Cu} = 0.1659$ (data are taken from [11]).

| Ion number | Ion type | | Cartesian coordinates | |
|---|---|---|---|---|
| 1 | Nd1 | 0 | $1/4$ | $z_{Nd}$ |
| 2 | Nd2 | 0 | $-1/4$ | $-z_{Nd}$ |
| 3 | Cu1 | 0 | $y_{Cu}$ | $z_{Cu}$ |
| 4 | Cu2 | 0 | $-y_{Cu}$ | $-z_{Cu}$ |
| 5 | Cu3 | 0 | $-1/2 + y_{Cu}$ | $-z_{Cu}$ |
| 6 | Cu4 | 0 | $1/2 - y_{Cu}$ | $z_{Cu}$ |
| | | | $+(1/2, 1/2, 1/2)$ | |

parameters ($y_{Cu}$, $z_{Cu}$, $z_{Nd}$) are free. The positions of the R- and Cu-ions in the unit cell are depicted in figure 1. The structure parameters are listed in table 1.

As the primitive cell consists of six ions, there are 18 phonon branches, which show no degeneracy along the three main symmetry directions. Nine of these branches are Raman active [21] at the Γ-point (a discussion of the lattice dynamics of the isostructural $YCu_2$ compound can be found in [19]).

### *3.2. Phonon dispersion relation*

Since there are 15 optical phonon branches within a comparatively narrow energy range of about 10 meV, additional information is needed to classify the measured phonons with respect to their symmetry. From the inelastic one-phonon neutron scattering cross section it follows that the structure factor depends on the scalar product of the scattering vector $\vec{\kappa}$ and the polarization

**Table 2.** Columns from left to right: bonding between the different Cu–Cu, Nd–Cu and Nd–Nd ions taken into account in the Born–von Karman model; a numbering of the springs indicated in figure 1 (odd numbers correspond to longitudinal, even numbers to transversal force constants); bonding length (length of the springs); longitudinal and transversal force constants. The arrangement is made according to increasing bonding length.

| Bond type | Spring number | Length (Å) | Longitudinal (N m$^{-1}$) | Transversal (N m$^{-1}$) |
|---|---|---|---|---|
| Cu1–Cu3 | 17/18 | 2.52 | 26.9 | −0.2 |
| Cu1–Cu2 | 19/20 | 2.56 | 27.3 | 5.7 |
| Cu1–Cu4 | 15/16 | 2.81 | 6.3 | 0.5 |
| Nd1–Cu2 | 13/14 | 3.01 | 27.4 | −2.2 |
| Nd1–Cu2 | 11/12 | 3.05 | 13.8 | −2.3 |
| Nd1–Cu1 | 9/10 | 3.10 | 21.5 | −2.2 |
| Nd1–Cu1 | 7/8 | 3.19 | 12.1 | 0.7 |
| Nd1–Nd2 | 5/6 | 3.56 | 31.8 | −3.7 |
| Nd1–Nd2 | 3/4 | 3.83 | 13.1 | −3.5 |
| Nd1–Nd1 | 1/2 | 4.39 | 12.2 | −2.8 |

vector of the phonon $\vec{\mathbf{e}}^{\vec{q}\nu,i}$ [19]. In the following we use $\vec{\kappa} = \vec{Q} + \vec{q}$, for a scattering vector in the extended zone scheme. The vector $\vec{Q}$ indicates the position of a zone centre ($\Gamma$-point) in the extended zone scheme and $\vec{q}$ is defined as a vector within a Brillouin zone. As the polarization vector is predetermined by the symmetry, one obtains information concerning the scattering intensity from symmetry considerations. Measurements performed at the same $\vec{q}$ and energy-range but in different Brillouin zones in the extended zone scheme, allowing the assignment of the peaks in the measured spectra to distinct phonon branches.

Experimental data are shown by symbols in figure 2. These data are received from constant-$q$ scans. For the low energy range of the acoustic phonons constant-energy scans have been performed. The error bars mark the full width at half maximum (FWHM) of the neutron peaks.

In order to calculate phonon dispersion relations a Born–von Karman model with 20 fitting parameters was applied. As starting parameters for the fit procedure the spring constants for $YCu_2$ given in [19] have been used. It follows from symmetry considerations that for each of the three main symmetry directions there exist four irreducible representations. For clarity, each of these representations is shown in a separate diagram in figure 2. The solid curves in the four diagrams of figure 2 show the phonon dispersion relations obtained from the Born–von Karman model fitted to the experimental data. The assignment of the experimental points to one of the four representations was done according to the local symmetry. The force constants obtained from the fit are given in table 2.

### *3.3. Phonon density of states*

The now known dispersion relation allows us to calculate the phonon density of states (PDOS). These results will now be compared with a measurement of the PDOS of $NdCu_2$ on a powdered sample material. We consider this procedure as a proof of the model calculation.

However, in order to compare the calculated phonon density of states with those obtained by the inelastic neutron scattering experiment, one should not simply count the number of phonons within a given energy range, but also calculate the neutron weighted PDOS. For this calculation the contributions of all scattering vectors $\vec{\kappa}$, allowed by geometric conditions in the scattering experiment, are summed up and corrected for the different scattering cross sections

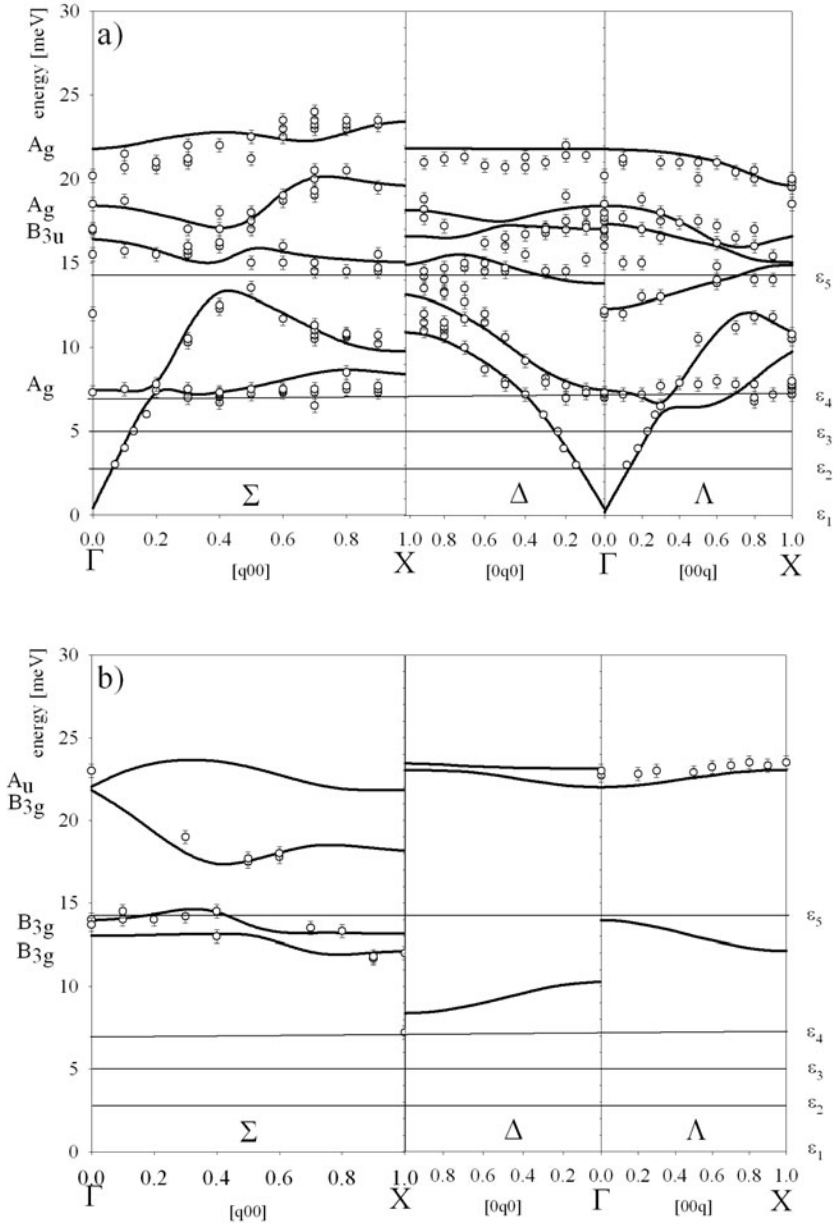


**Figure 2.** Phonon dispersion relation of $NdCu_2$. The four pictures (a)–(d) represent the four irreducible representations. Each picture is divided into three sections showing the three main symmetry directions. The symbols give the peak positions of the neutron scattering experiments. The curves are the result of the Born–von Karman fit procedure. The horizontal lines ($\varepsilon_\gamma$) mark the positions of the CEF levels.

in various shells of Brillouin zones with $|\vec{\kappa}| = \text{constant}$

$$g(\omega) = \sum_{\vec{\kappa}} \frac{\omega}{\kappa^2} \frac{1}{n(\omega)+1} \left( \frac{\mathrm{d}^2\sigma}{\mathrm{d}\Omega\, \mathrm{d}\omega} \right)_{\text{coh}}^{\text{inel}} \tag{1}$$

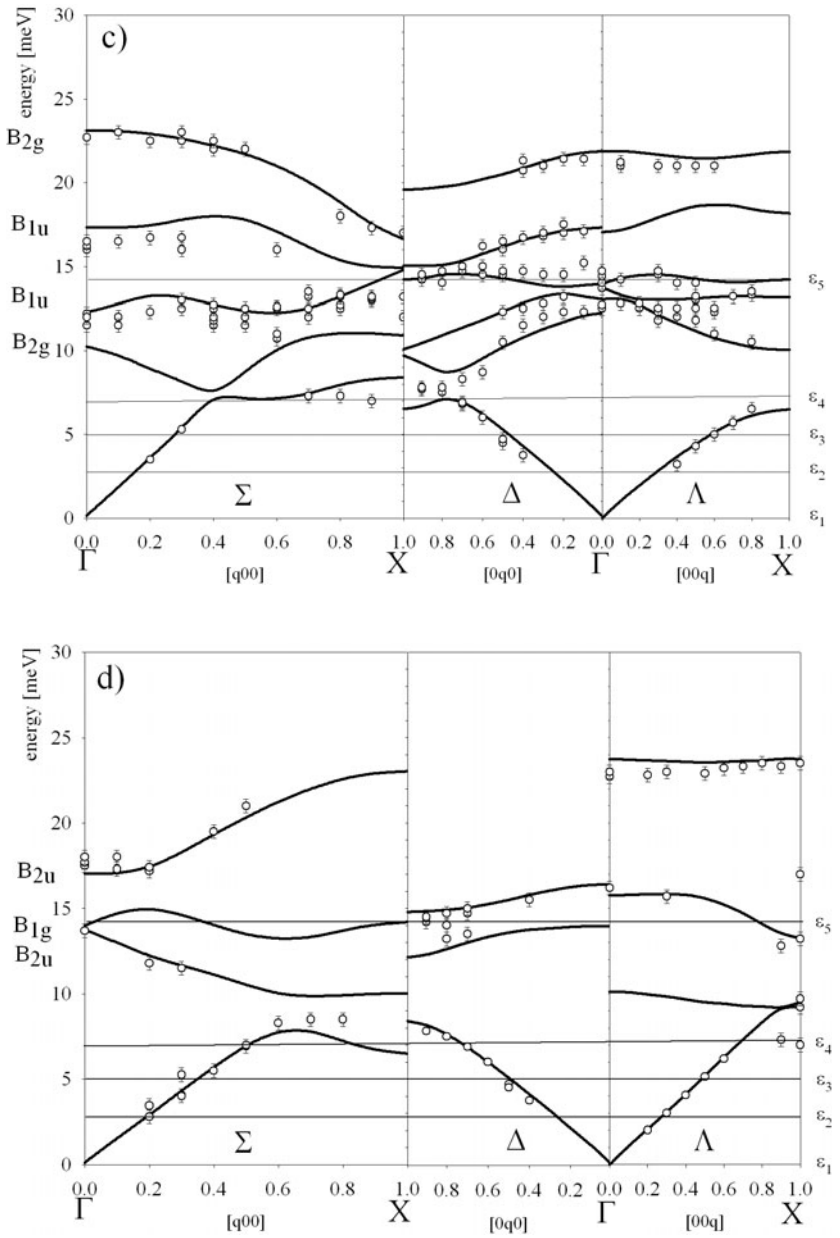


**Figure 2.** (Continued.)

with the one phonon inelastic coherent scattering cross section (see also [30]):

$$\left(\frac{\mathrm{d}^2\sigma}{\mathrm{d}\Omega\,\mathrm{d}\omega}\right)_{\mathrm{coh}}^{\mathrm{inel}} = \frac{k_f}{k_i}\frac{(2\pi)^3}{V}\sum_{\vec{Q}}\sum_{\vec{q}\nu}\delta(\vec{Q}+\vec{q}-\vec{\kappa})|H_{\vec{q}\nu}(\vec{\kappa})|^2 S_{\vec{q}\nu}(\omega) \tag{2a}$$

$$S_{\vec{q}\nu}(\omega) = \frac{1}{2\omega_{\vec{q}\nu}}\{n_{\vec{q}\nu}\delta(\omega+\omega_{\vec{q}\nu}) + (1+n_{\vec{q}\nu})\delta(\omega-\omega_{\vec{q}\nu})\} \tag{2b}$$

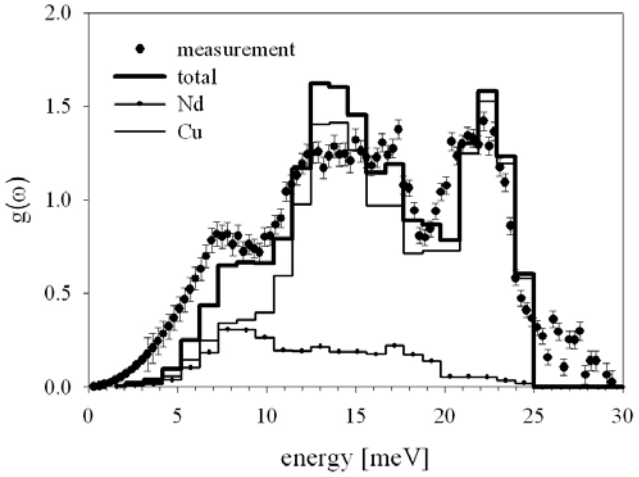


**Figure 3.** Phonon density of states (PDOS) of $NdCu_2$. The symbols show the results of the time of flight experiment. The histograms are the results of the neutron weighted PDOS calculations based on the Born–von Karman model.

$$H_{\vec{q}\nu}(\vec{\kappa}) = \sum_i \frac{\bar{b}_i}{\sqrt{M_i}} \mathrm{e}^{-W_i(\vec{\kappa})} \mathrm{e}^{\mathrm{i}\vec{\kappa}\cdot\vec{R}_i} \{\vec{\kappa}\cdot\vec{\mathbf{e}}^{\vec{q}\nu,i}\}. \tag{2c}$$

The $\sum_{\vec{Q}}$ is a sum over all reciprocal lattice vectors, the index $\nu$ is used to distinguish between different phonon branches. The phonon frequency and the polarization vector are $\omega_{\vec{q}\nu}$ and $\vec{\mathbf{e}}^{\vec{q}\nu,i}$, respectively. The first part in equation (2*b*) is the contribution of phonon annihilation, whereas the second accounts for phonon creation. The term $\mathrm{e}^{-W_i(\vec{\kappa})}$ is the Debye–Waller factor, which, however, will be neglected in the following.

In figure 3, the experimental data and the calculated neutron weighted PDOS are shown. Taking into account only the contribution of a specific sort of ion (Nd or Cu), it is possible to calculate the partial density of states. As can be seen in figure 3 the general feature of the measured PDOS is satisfactorily reproduced by the calculation. The low energy part of the experimental data set has been cancelled because of difficulties in correcting the quasi elastic contribution to the spectra, as well as the incoherent scattering. Therefore, the data set was completed by a quadratic relation down to zero energy.

## 4. Crystal electric field excitations

### *4.1. Crystal electric field Hamiltonian*

The local symmetry of the ions ($Nd^{3+}$) in the $CeCu_2$-type structure is $C_{2v}$. Therefore, nine CEF parameters are nonzero [22]. As $Nd^{3+}$ has a $^4I_{9/2}$ ground-state, the CEF splits it into five Kramers doublets.

The description of the CEF used in this work is based on a point charge model [24]. The ions within one primitive unit cell $n'$ are enumerated by the index $i'$. The undisturbed position of the ion $i'$ in the cell $n'$ is given by $\vec{R}_{n'i'}$. The difference vector between two ions at the position $\vec{R}_{ni}$ and $\vec{R}_{n'i'}$ is:

$$\vec{R}_{n'i',ni} = \vec{R}_{n'i'} - \vec{R}_{ni}. \tag{3}$$

The potential seen by the ion $ni$ is $V^0_{ni}(\vec{r})$, whereby $\vec{r} = 0$ always corresponds to the position $\vec{R}_{ni}$ of the ion under consideration. It is caused by all the surrounding ions at the

**Table 3.** Comparison of the CEF parameters $\sigma_m^\alpha$ deduced from the experiment ($\sigma_{m\alpha}^{\mathrm{exp}}$) [11] and calculated from a point charge model ($\sigma_{m\alpha}^{\mathrm{PCM}}$). In order to quantify the agreement of both values the ratio $S_{m\alpha}$ is given in the last column. The charge of Nd and Cu was chosen to be $q_{\mathrm{Nd}} = 0.33e$ and $q_{\mathrm{Cu}} = -0.165e$, respectively ($e = 1.6 \times 10^{-19}$ C). The Nd-ion parameters used for the point charge model calculation are: $\langle r^2 \rangle = 0.312$ Å$^2$, $\langle r^4 \rangle = 0.2282$ Å$^4$, $\langle r^6 \rangle = 0.3300$ Å$^6$, $\lambda_2 = -0.643 \times 10^{-2}$, $\lambda_4 = -2.91 \times 10^{-4}$, $\lambda_6 = -38 \times 10^{-6}$ [23].

| CEF parameter | $\sigma_{m\alpha}^{\mathrm{exp}}$ (K) | $\sigma_{m\alpha}^{\mathrm{PCM}}$ (K) | $\mathcal{S}_{m\alpha}$ |
|---|---|---|---|
| $\sigma_2^0$ | $1.35 \times 10^{0}$ | $1.78 \times 10^{0}$ | 0.758 |
| $\sigma_2^2$ | $1.56 \times 10^{0}$ | $2.31 \times 10^{0}$ | 0.675 |
| $\sigma_4^0$ | $2.23 \times 10^{-2}$ | $1.37 \times 10^{-2}$ | 1.628 |
| $\sigma_4^2$ | $1.01 \times 10^{-2}$ | $1.38 \times 10^{-2}$ | 0.732 |
| $\sigma_4^4$ | $1.96 \times 10^{-2}$ | $-2.75 \times 10^{-3}$ | −7.127 |
| $\sigma_6^0$ | $5.52 \times 10^{-4}$ | $2.81 \times 10^{-4}$ | 1.964 |
| $\sigma_6^2$ | $1.35 \times 10^{-4}$ | $-1.03 \times 10^{-4}$ | −1.301 |
| $\sigma_6^4$ | $4.89 \times 10^{-4}$ | $-2.21 \times 10^{-4}$ | −2.213 |
| $\sigma_6^6$ | $4.25 \times 10^{-3}$ | $-5.29 \times 10^{-5}$ | −80.34 |

positions $\vec{R}_{n'i'}$ with the point charges $q_{i'}$ and is given by:

$$V_{ni}^0(\vec{r}) = \sum_{n'i'(\neq ni)} \frac{q_{i'}}{|\vec{R}_{n'i',ni} - \vec{r}|}, \tag{4a}$$

$V_{ni}^0(\vec{r})$ has the symmetry of the site of the ion $ni$. This potential can be expanded in terms of spherical harmonics (or tesseral harmonics $Z_{m\alpha} = [Y_m^{-\alpha} + (-1)^\alpha Y_m^\alpha]/\sqrt{2}$ in order to avoid imaginary quantities). Using the usual expanding formula for $1/R$, the potential $V_{ni}^0$ is now given by:

$$V_{ni}^0(r, \Theta, \phi) = \sum_{m=0}^{\infty} r^m \sum_{\alpha=-m}^{m} \underbrace{\sum_{n'i'(\neq ni)} \frac{q_{i'}}{R_{n'i',ni}^{m+1}} \frac{4\pi}{(2m+1)} Z_{m\alpha}(\Theta_{n'i',ni}, \phi_{n'i',ni})}_{(\gamma_{m\alpha}^{ni})^0} Z_{m\alpha}(\Theta, \phi) \tag{4b}$$

where $(\gamma_{m\alpha}^{ni})^0$ depends only on the local symmetry of the ion under consideration. Using this method, the undisturbed CEF Hamiltonian for the ion $ni$ can be written as:

$$\mathcal{H}_{\mathrm{CEF}}^0(ni) = \sum_{m\alpha} (\gamma_{m\alpha}^{ni})^0 \langle r^m(i) \rangle \lambda_m O_m^\alpha(ni) = \sum_{m\alpha} \sigma_m^\alpha(ni)\, O_m^\alpha(ni) \tag{5}$$

where the $\lambda_m$ are numerical factors occurring in Stevens operators equivalents and $\sigma_m^\alpha$ are the CEF parameters. The experiment allows an estimation of these CEF parameters by fitting the calculated magnetic scattering cross section to measured neutron data. The CEF parameters obtained in this way by Gratz *et al* [11] for $NdCu_2$ are given in column $\sigma_{m\alpha}^{\mathrm{exp}}$ of table 3, the results of a point charge model calculation in column $\sigma_{m\alpha}^{\mathrm{PCM}}$. A calculation of CEF parameters based on the assumption that the charges are located at the position of the nuclei of the surrounding ions is a rough approximation for metals where the shielding-effect of the conduction electrons can hardly be neglected. The discrepancies between the point charge model calculation and the experimental determined CEF parameters is quantified by the ratio $\mathcal{S}_{m\alpha}$ in the last column of table 3. In the calculation of the CEF–phonon interaction these $\mathcal{S}_{m\alpha}$-values are used as scaling factors.

**Table 4.** Comparison of the measured CEF energy levels and those calculated using the point charge model.

| $\varepsilon_\gamma$ | Measured (meV) | Calculated (meV) |
|---|---|---|
| $\varepsilon_5$ | 14.1 | 13.6 |
| $\varepsilon_4$ | 7.2 | 7.0 |
| $\varepsilon_3$ | 5.0 | 5.2 |
| $\varepsilon_2$ | 2.9 | 2.5 |
| $\varepsilon_1$ | 0.0 | 0.0 |

The total CEF Hamiltonian of the undisturbed crystal is given by the sum of the Hamiltonians of each ion

$$\mathcal{H}^0_{\mathrm{CEF}} = \sum_{ni} \mathcal{H}^0_{\mathrm{CEF}}(ni). \tag{6a}$$

This total Hamiltonian can also be written in terms of the eigenstates of the Hamiltonian or in second quantization using fermion-creation and -annihilation operators:

$$\mathcal{H}^0_{\mathrm{CEF}} = \sum_{ni}\sum_{\gamma} |\gamma, ni\rangle(\varepsilon^{ni}_\gamma + \mu^{ni})\langle\gamma, ni| = \sum_{ni}\sum_{\gamma}(\varepsilon^{ni}_\gamma + \mu^{ni})c^\dagger_\gamma(ni)c_\gamma(ni) \tag{6b}$$

where $\varepsilon^{ni}_\gamma$ denotes the energy of the crystal field level $\gamma$ of the ion $ni$. The $c^\dagger_\gamma(ni)$ and $c_\gamma(ni)$ are fermion-creation and -annihilation operators for the site $ni$. The chemical potential is denoted by $\mu^{ni}$. For a description of the second quantization of fermion states see [25].

In table 4 the experimental data for $\varepsilon_\gamma$ obtained at 10 K (see [11]) are compared with the calculated $\varepsilon_\gamma$-values based on the point charge model.

### *4.2. Experimental evidence for the CEF–phonon interaction*

From table 4 it follows that the CEF excitation energies range from about 3 meV up to 14 meV, which is about the same as the 10 meV energy interval, where all the optical phonon branches of $NdCu_2$ exist. This is an important prerequisite for a measurable CEF–phonon interaction.

An indication for the existence of the CEF–phonon interaction observable in the neutron experiment is shown in figure 4. In this diagram the normalized peak intensities $I_{(0\kappa 0)}/I_{(020)}$ of the $\varepsilon_3$ (5.0 meV) and the $\varepsilon_4$ (7.2 meV) CEF excitations as a function of the length of the scattering vector $\vec{\kappa}$ in the $b$-direction are given. From the theory it follows that the neutron peak intensity for scattering due to CEF excitations (magnetic scattering) decreases monotonically with increasing $\vec{\kappa}$. This is indeed the case for the $\varepsilon_3$ CEF excitation. The same tendency exists for the $\varepsilon_4$ (7.2 meV) CEF excitation, however, with the exception for $\kappa = 4$. The enlarged intensity at (040) can be understood as caused by the additional CEF–phonon interaction, which will be considered in the following section. This observation was a first hint that the $\varepsilon_4$ CEF excitation might be a possible candidate for a measurable interaction effect between the CEF and the phonons.

At the beginning of the following section the concept model used for the discussion of the CEF–phonon interaction will be outlined. A quantitative discussion of the influence of the phonons on the $\varepsilon_4$ CEF level follows. Finally the influence of the CEF on phonon modes is considered.

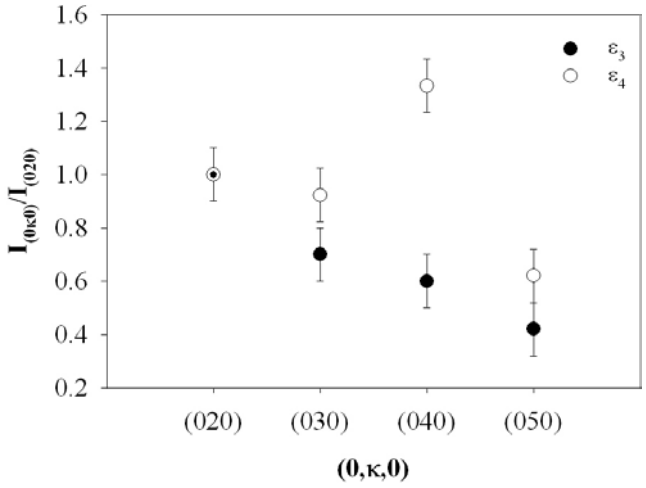


**Figure 4.** Neutron peak intensity of the $\varepsilon_3$ (•) and the $\varepsilon_4$ (○) CEF excitations measured at 50 K along the *b*-direction at (020), (030), (040) and (050). Data are scaled to the (020) intensity.

## 5. CEF–phonon interaction

### *5.1. Interaction Hamiltonian*

When allowing the ions $n'i'$ to be shifted by a displacement vector $\vec{u}_{n'i'}$ with respect to their equilibrium position the potential in equation (4*a*) has to be modified taking into account the corresponding displacement

$$V_{ni}(\vec{r}) = \sum_{n'i'(\neq ni)} \frac{q_{i'}}{|(\vec{R}_{n'i'} + \vec{u}_{n'i'}) - (\vec{R}_{ni} + \vec{u}_{ni}) - \vec{r}|}. \tag{7}$$

Consequently $(\gamma_{m\alpha}^{ni})^0$ in equation (4*b*) is changed to $\gamma_{m\alpha}^{ni}$ depending on $\vec{u}_{ni}$. Using the Taylor series expansion

$$\gamma_{m\alpha}^{ni}(\vec{u}) = \gamma_{m\alpha}^{ni}\Big|_{\vec{u}=0} + \sum_{n'i'} \sum_{l=1}^{3} \left( \frac{\partial \gamma_{m\alpha}^{ni}}{\partial (\vec{u}_{n'i'})_l} \right)_{\vec{u}=0} (\vec{u}_{n'i'})_l + \cdots \tag{8}$$

the first order expansion term is usually used for the description of the interaction. When dealing with the interaction of phonons with the CEF, the displacement is due to the lattice vibrations

$$(u_{n'i'})_l = \sqrt{\frac{1}{2NM_{i'}}} \sum_{\vec{q}\nu} \sqrt{\frac{1}{\omega_{\vec{q}\nu}}} \mathbf{e}_l^{\vec{q}\nu,i'} \mathrm{e}^{\mathrm{i}\vec{q}\,\vec{R}_{n'i'}} (a_{-\vec{q}\nu}^{\dagger} + a_{\vec{q}\nu}), \tag{9}$$

where the energy of a phonon belonging to the branch $\nu$ with wavevector $\vec{q}$ is given by $\omega_{\vec{q}\nu}$. The sum over $\vec{q}$ had to be done for all wavevectors inside the first Brillouin zone. The $l$-component of the polarization vector of ion $i'$ of the phonon $\vec{q}\nu$ is given by $\mathbf{e}_l^{\vec{q}\nu,i'}$. The $a_{-\vec{q}\nu}^{\dagger}$ and $a_{\vec{q}\nu}$ are boson-creation and -annihilation operators, respectively.

Using equation (9), equation (8) can be written as:

$$\gamma_{m\alpha}^{ni} = (\gamma_{m\alpha}^{ni})^0 + \frac{1}{\sqrt{N}} \sum_{\vec{q}\nu} \underbrace{\sum_{n'i'} \sum_{l=1}^{3} \sqrt{\frac{1}{2M_{i'}\omega_{\vec{q}\nu}}} \left( \frac{\partial \gamma_{m\alpha}^{ni}}{\partial (\vec{u}_{n'i'})_l} \right)_{\vec{u}=0} \mathbf{e}_l^{\vec{q}\nu,i'} \mathrm{e}^{\mathrm{i}\vec{q}\,\vec{R}_{n'i'}}}_{A_{m\alpha}^{\vec{q}\nu,ni}} (a_{-\vec{q}\nu}^{\dagger} + a_{\vec{q}\nu}). \tag{10}$$

The CEF Hamiltonian including the interaction with the phonons is now given by

$$\mathcal{H}_{\mathrm{CEF}}(ni) = \mathcal{H}^0_{\mathrm{CEF}}(ni) + \frac{1}{\sqrt{N}} \sum_{\vec{q}\nu} \sum_{m\alpha} \mathcal{V}^{\vec{q}\nu,i}_{m\alpha} (a^{\dagger}_{-\vec{q}\nu} + a_{\vec{q}\nu}) O^{\alpha}_{m}(ni) \tag{11}$$

with the interaction strength

$$\mathcal{V}^{\vec{q}\nu,i}_{m\alpha} = \langle r^m(i) \rangle \lambda_m \mathcal{A}^{\vec{q}\nu,ni}_{m\alpha}. \tag{12}$$

In second quantization the total Hamiltonian of the interacting system of phonons and CEF excitations reads

$$\mathcal{H} = \mathcal{H}^0_{\mathrm{phon}} + \mathcal{H}^0_{\mathrm{CEF}} + \mathcal{H}_{\mathrm{int}} = \sum_{\vec{q}\nu} \omega_{\vec{q}\nu} (a^{\dagger}_{\vec{q}\nu} a_{\vec{q}\nu} + \tfrac{1}{2}) + \sum_{\gamma,ni} (\varepsilon^{ni}_{\gamma} + \mu^{ni}) c^{\dagger}_{\gamma}(ni) c_{\gamma}(ni)$$
$$+ \frac{1}{\sqrt{N}} \sum_{\gamma',\gamma} \sum_{\vec{q}\nu} \sum_{m\alpha,ni} \mathcal{V}^{\vec{q}\nu,i}_{m\alpha} \underbrace{\langle \gamma', ni | O^{\alpha}_{m} | \gamma, ni \rangle}_{O^{\alpha}_{m}(\gamma',\gamma)} (a^{\dagger}_{-\vec{q}\nu} + a_{\vec{q}\nu}) c^{\dagger}_{\gamma'}(ni) c_{\gamma}(ni). \tag{13}$$

The interaction Hamiltonian $\mathcal{H}_{\mathrm{int}}$ causes the system to make transitions from the state $|\gamma\rangle \otimes |\{n_{\vec{q}\nu}\}\rangle$ to the state $|\gamma'\rangle \otimes |\{n_{\vec{q}\nu}\} \pm 1_{\vec{q}\nu}\rangle$, meaning that the CEF state changes from $\gamma \to \gamma'$, and one phonon $\vec{q}\,\nu$ is created or annihilated. The interaction strength $\mathcal{V}^{\vec{q}\nu,i}_{m\alpha}$ contains the symmetry of the lattice-distortion caused by the phonon $\vec{q}\,\nu$. It is obvious, that all possible symmetries of distortions are contained in the irreducible representations of the group of the site symmetry of the ion. This is equivalent to the fact, that the operator $\sum_{m\alpha} \mathcal{V}^{\vec{q}\nu,i}_{m\alpha} O^{\alpha}_{m}$ has to transform according to an irreducible representation of the group of the site symmetry of the ion under consideration. According to Eyring *et al* [21], the representations of the point group $C^{z}_{2v}$ are labelled $A_1$; $A_2$; $B_1$ and $B_2$. They transform like the coordinates ($x^2$, $y^2$ and $z^2$) $xy$; $xz$ and $yz$, respectively. When using Stevens operator equivalents, the Cartesian coordinates can be replaced by the corresponding coordinates of the angular momentum operator.

Using the method given by Herzfeld and Meijer [26], one finds that only phonons causing distortions of local symmetry $A_1$ are capable of coupling to the CEF. This method is an application of the fact that the distorted CEF cannot lift the Kramers degeneracy. Therefore, the coupling strength has to be zero for coupling-operators (produced by symmetry considerations) causing the Kramers degenerated states to split.

The Γ-point phonons capable of coupling to the CEF belong to the irreducible representation $A_g$ (see also [27]). It is important to note that, from symmetry considerations, one gets only the phonons that might couple. However, the coupling strength can be so small that the interaction is not measurable.

### *5.2. Calculation of neutron scattering functions*

For the calculation of the neutron–phonon and the neutron–CEF scattering functions, the Matsubara Green functions formalism in the random phase approximation (RPA) [3, 28, 29] will be used. The self energy operators $\Sigma_C$ for the electrons and $\Sigma_Q$ for the phonons occurring in Dysons equations

$$G = G_0 + G_0 \Sigma_C G \qquad \text{or} \qquad G^{-1} = G_0^{-1} - \Sigma_C$$
$$\text{with } G_0(\gamma, \omega) = \frac{1}{\omega - \varepsilon_{\gamma} + i\eta^{0+}} \tag{14a}$$
$$D = D_0 + D_0 \Sigma_Q D \qquad \text{or} \qquad D^{-1} = D_0^{-1} - \Sigma_Q$$
$$\text{with } D_0(\vec{q}\nu, \omega) = \frac{\omega_{\vec{q}\nu}}{\omega^2 - \omega^2_{\vec{q}\nu} + i\eta^{0+}} \tag{14b}$$

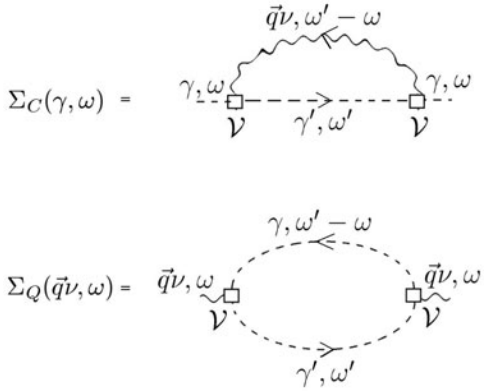


**Figure 5.** Feynman graphs for the self energies $\Sigma_C$ and $\Sigma_Q$ in the random phase approximation. Dashed lines correspond to $G_0$ and wavy lines to $D_0$.

reveal the energy shift and damping due to the interaction Hamiltonian $\mathcal{H}_{\rm int}$. $G$ and $D$ are the Green functions for the electrons and phonons, respectively. The undisturbed Green functions are denoted by $G_0$ and $D_0$.

The Feynman diagrams for the self energies $\Sigma_C$ and $\Sigma_Q$ are depicted in figure 5.

The evaluation of these diagrams reveals for the electron self energy

$$\Sigma_C(\gamma,\omega) = \Sigma_C^1(\gamma,\omega) + i\,\Sigma_C^2(\gamma,\omega) \tag{15a}$$

$$\Sigma_C^1(\gamma,\omega) = \frac{1}{N}\sum_{\vec{q}\nu}\sum_{\gamma'}\left|\sum_{m\alpha}\mathcal{V}_{m\alpha}^{\vec{q}\nu}O_m^\alpha(\gamma,\gamma')\right|^2\left(\frac{n_{\vec{q}\nu}-p_{\gamma'}}{\omega-\varepsilon_{\gamma'}+\omega_{\vec{q}\nu}}+\frac{n_{\vec{q}\nu}+1+p_{\gamma'}}{\omega-\varepsilon_{\gamma'}-\omega_{\vec{q}\nu}}\right) \tag{15b}$$

$$\begin{aligned}\Sigma_C^2(\gamma,\omega) = \frac{1}{N}\sum_{\vec{q}\nu}\sum_{\gamma'}\left|\sum_{m\alpha}\mathcal{V}_{m\alpha}^{\vec{q}\nu}O_m^\alpha(\gamma,\gamma')\right|^2((n_{\vec{q}\nu}-p_{\gamma'})\delta(\omega-\varepsilon_{\gamma'}+\omega_{\vec{q}\nu})\\ -(n_{\vec{q}\nu}+1+p_{\gamma'})\delta(\omega-\varepsilon_{\gamma'}-\omega_{\vec{q}\nu}))\end{aligned} \tag{15c}$$

where the following abbreviations are used:

$$n_{\vec{q}\nu} = \frac{1}{\mathrm{e}^{\omega_{\vec{q}\nu}/k_{\rm B}T}-1}, \qquad p_\gamma = Z_0^{-1}\exp\left(\frac{-\varepsilon_\gamma}{k_{\rm B}T}\right), \qquad Z_0 = \sum_\gamma \exp\left(\frac{-\varepsilon_\gamma}{k_{\rm B}T}\right). \tag{16}$$

$\Sigma_C^1$ is the real part and $\Sigma_C^2$ the imaginary part of the self energy $\Sigma_C$. With equations (14*a*) and the self energy operator, the electron Green function of the disturbed system (in RPA) is given by:

$$G(\gamma,\omega) = (\omega-\varepsilon_\gamma-\Sigma_C)^{-1} = (\omega-\varepsilon_\gamma-\Sigma_C^1-i\,\Sigma_C^2)^{-1}. \tag{17}$$

The corresponding neutron scattering function, $S_C(\gamma,\omega)$, for the CEF excitations is determined by the imaginary part of the Green function $G$. This expression reads:

$$S_C(\gamma,\omega) = \frac{\Sigma_C^2(\gamma,\omega)}{(\omega-\varepsilon_\gamma-\Sigma_C^1(\gamma,\omega))^2+(\Sigma_C^2(\gamma,\omega))^2}. \tag{18}$$

The CEF–phonon interactions also change the phonon properties. Treating the phonon self energy in the same way as the electron self energy, the phonon self energy $\Sigma_Q$ can similarly be separated into real and imaginary parts:

$$\Sigma_Q(\vec{q}\nu,\omega) = \Sigma_Q^1(\vec{q}\nu,\omega) + i\,\Sigma_Q^2(\vec{q}\nu,\omega) \tag{19a}$$

**Table 5.** Interaction strength $\mathcal{V}_{m\alpha}^{\vec{q}\nu}$ for the 7.5 meV $A_g$-mode at the Γ-point given in units of kelvin.

| | $\alpha$ | | | |
|---|---|---|---|---|
| $m$ | 0 | 2 | 4 | 6 |
| 2 | $8.68 \times 10^{-1}$ | $-9.17 \times 10^{-1}$ | | |
| 4 | $3.26 \times 10^{-4}$ | $-1.42 \times 10^{-2}$ | $1.09 \times 10^{-3}$ | |
| 6 | $1.64 \times 10^{-4}$ | $2.27 \times 10^{-4}$ | $1.70 \times 10^{-4}$ | $1.40 \times 10^{-4}$ |

$$\Sigma_Q^1(\vec{q}\nu,\omega) = \sum_{\gamma,\gamma'} \left| \sum_{m\alpha} \mathcal{V}_{m\alpha}^{\vec{q}\nu} O_m^\alpha(\gamma',\gamma) \right|^2 \frac{p_{\gamma'} - p_\gamma}{\omega - \varepsilon_\gamma + \varepsilon_{\gamma'}} \tag{19b}$$

$$\Sigma_Q^2(\vec{q}\nu,\omega) = -\sum_{\gamma,\gamma'} \left| \sum_{m\alpha} \mathcal{V}_{m,\alpha}^{\vec{q}\nu} O_m^\alpha(\gamma',\gamma) \right|^2 \delta(\omega - \varepsilon_\gamma + \varepsilon_{\gamma'})(p_{\gamma'} - p_\gamma). \tag{19c}$$

The neutron scattering function for the phonon subsystem $S_Q(\vec{q}\nu,\omega)$ is given by the imaginary part of the phonon Green function $D$ (equation (14*b*)):

$$S_Q(\vec{q}\nu,\omega) = \frac{\omega_{\vec{q}\nu}^2 \Sigma_Q^2(\vec{q}\nu,\omega)}{(\omega^2 - \omega_{\vec{q}\nu}^2 - \omega_{\vec{q}\nu}\Sigma_Q^1(\vec{q}\nu,\omega))^2 + \omega_{\vec{q}\nu}^2(\Sigma_Q^2(\vec{q}\nu,\omega))^2}. \tag{20}$$

Equations (18) and (20) will be used for the analysis of experimental data of $NdCu_2$. For this discussion it is important to note that the measured line width as well as the line position in both subsystems (CEF and phonons) are temperature dependent due to the terms $n_{\vec{q}\nu}$ and $p_\gamma$ occurring in equations (15*b*), (15*c*), (19*b*) and (19*c*).

## 6. Influence of the CEF–phonon interaction

### *6.1. Calculation of the interaction strength*

The neutron scattering functions are determined by the self energies $\Sigma_C$ and $\Sigma_Q$, which depend on the total interaction strength $|\sum_{m\alpha} \mathcal{V}_{m\alpha}^{\vec{q}\nu} O_m^\alpha(\gamma,\gamma')|^2$. We first have to calculate the interaction strength $\mathcal{V}_{m\alpha}^{\vec{q}\nu}$ (see equation (12); no index $i$ is needed because all Nd-ions are equivalent). In order to calculate $\mathcal{V}_{m\alpha}^{\vec{q}\nu}$, it is necessary to know the polarization vector of the phonon under consideration. This vector is given by the solution of the Born–von Karman model (see [19]).

From table 3 it follows that there are discrepancies between the CEF parameters obtained from the experiment and those from the point charge model (PCM) calculation. This is why the scaling parameters $S_{m\alpha}$ ($\sigma_{m\alpha}^{\mathrm{exp}} = \mathcal{S}_{m\alpha}\sigma_{m\alpha}^{\mathrm{PCM}}$) have been introduced. The calculation was done in the scope of the point charge model using the displacements from the Born–von Karman model and then the thus obtained interaction strength was scaled with the corresponding $S_{m\alpha}$-value.

The interaction strength $\mathcal{V}_{m\alpha}^{\vec{q}\nu}$ obtained in this way at the Γ-point for the 7.5 meV $A_g$-mode are given in table 5.

Values of $\mathcal{V}_{m\alpha}^{\vec{q}\nu}$ for other $\vec{q}$-vectors and $\nu$-values have been obtained by the same procedure. For the calculation of the total interaction strength we further need the matrix elements of the Stevens operator equivalents between CEF eigenstates: $O_m^\alpha(\gamma,\gamma')$. As an example, values of the total interaction strength for the mode under consideration are given in table 6. In this table values are given only for five CEF states $\gamma$ although there are in total 10 CEF states in the $Nd^{3+}$-ion. As the states are degenerated (Kramers degeneration), there exist for each state $\gamma$ a state $\tilde{\gamma}$ with the same energy. Only the matrix elements between the five states $\gamma$ are given.

**Table 6.** Total interaction strength $|\sum_{m\alpha} \mathcal{V}^{\vec{q}\nu}_{m\alpha} O^{\alpha}_{m}(\gamma, \gamma')|^2$ for the 7.5 meV $A_g$-mode at the Γ-point given in units of $K^2$.

| | $\gamma'$ | | | | |
|---|---|---|---|---|---|
| $\gamma$ | 5 | 4 | 3 | 2 | 1 |
| 5 | 895 | 37.4 | 115 | 48.3 | 19 |
| 4 | 37.4 | 621.4 | 0.48 | 74.1 | 59.8 |
| 3 | 115 | 0.48 | 85.2 | 22.4 | 179.3 |
| 2 | 48.3 | 74.1 | 22.4 | 33.1 | 25.1 |
| 1 | 19 | 59.8 | 179.3 | 25.1 | 2.31 |

The matrix elements between one of the five states $\gamma$ and one of the five states $\tilde{\gamma}$ vanish and the matrix element between two states out of the five states $\tilde{\gamma}$ are equal to the matrix element between the corresponding $\gamma$-states.

### *6.2. Influence of the CEF–phonon interaction on the CEF excitations*

As a consequence of the CEF–phonon interaction on the CEF-spectra a pronounced temperature dependent shift and broadening of the CEF level in the neutron spectra is expected. In order to select these CEF level where the shift and broadening is strongest and therefore most exactly measurable, we consider the neutron scattering function (equation (18)). A measure for the broadening and the shift is given by the terms $\Sigma^2_C$ (equation (15*c*)) and $\Sigma^1_C$ (equation (15*b*)). Both functions include a sum over all the $\vec{q}$-vectors inside the first Brillouin zone and the phonon branches $\nu$. The summation can, however, be limited to those phonon modes able to couple to the CEF level (as mentioned above these are the $A_g$ modes). Furthermore the influence of the interaction strength will be significant only if $\varepsilon_\gamma + \omega_{\vec{q},\nu} \sim \omega$ for phonon creation or $\varepsilon_\gamma - \omega_{\vec{q},\nu} \sim \omega$ for phonon annihilation. An inspection of figure 2 immediately shows that there is one ideal configuration where these necessary conditions for the observation of the CEF–phonon interaction are ideally fulfilled. This is the $\varepsilon_4$ CEF level and the 7.5 meV $A_g$-phonon mode in the neighbourhood of the zone centre.

For the discussion of the experimental data it is important to note that due to the CEF–phonon interaction, a temperature dependent shift and broadening of the measured CEF level is the consequence of this interaction. In equations (15*b*) and (15*c*) as well as in equations (19*b*) and (19*c*) the terms $n_{\vec{q}\nu}$ and $p_\gamma$ reflect this temperature dependency.

In order to determine the CEF–phonon interaction strength we investigated the temperature dependence of the shift and broadening of the $\varepsilon_4$. Figure 6 shows the neutron line shape in the vicinity of the $\varepsilon_4$ CEF level at different temperatures. The (020) Γ-point was used for these measurements since the neutron scattering vector $\kappa$ is small there, which means that the measured intensity is predominantly due to the CEF scattering. Simultaneously we also studied the temperature dependence of the shift of the $\varepsilon_5$ CEF level at the (020) Γ-point (the $\varepsilon_5$ CEF level is well separated from its nearest $A_g$-phonon mode (see figure 2); a shift of this level will hardly be due to the CEF–phonon interaction).

Difficulties in the quantitative determination of the line broadening result from the fact that there are two further mechanisms giving rise to a broadening. One is caused by the electron–electron interaction [23] and another due to the spectrometer function (specific for the experimental facility used). Therefore in the following we will not further analyse the line broadening but consider the line shift and compare it with the theory.

Details of the fit procedure: to get the absolute value of the temperature dependence of the line shift due the CEF–phonon interaction we replace $\eta^{0+}$ in equation (14*a*) by a finite line

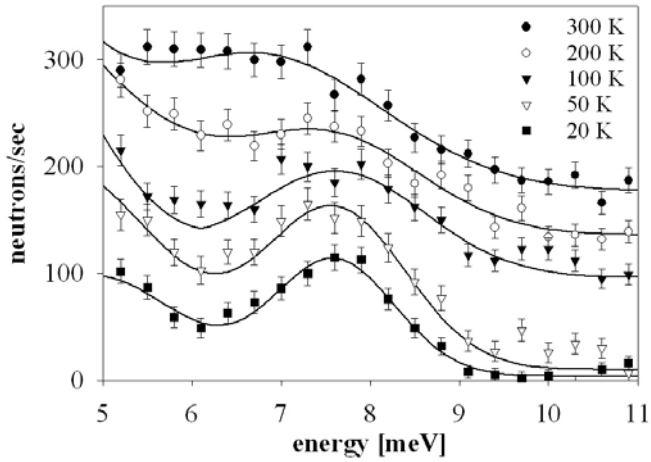


**Figure 6.** Neutron scattering intensity in the vicinity of the $\varepsilon_4$-CEF level measured at the (020) Γ-point at different temperatures.

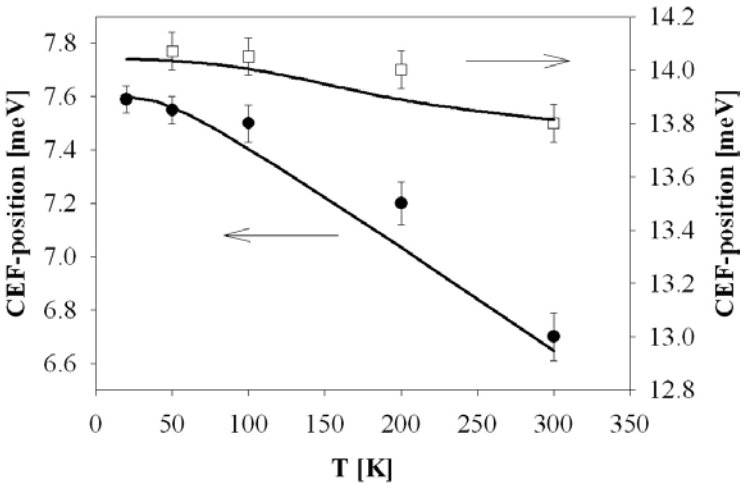


**Figure 7.** Temperature dependent shift of the centre of gravity of the $\varepsilon_4$ CEF level (•) and the $\varepsilon_5$ CEF level (□) both measured at the (020) Γ-point. The lines represent the calculation (see the text).

width Δ, i.e. we replace in equation (15*b*):

$$\frac{1}{\omega - E} \rightarrow \frac{\omega - E}{(\omega - E)^2 + \Delta^2} \tag{21}$$

where $E$ is an abbreviation for $(\varepsilon_{\gamma'} - \omega_{\vec{q}\nu})$ or $(\varepsilon_{\gamma'} + \omega_{\vec{q}\nu})$. The used value of Δ was 0.9 meV (deduced from the experimental data). The temperature shift for the $\varepsilon_4$ and $\varepsilon_5$ CEF level are compared in figure 7. To test whether the temperature variation of the shift of the $\varepsilon_4$-level given by (•)-symbols can be described by equation (15*b*); this has been fitted to the data. As can be seen there is a quite good qualitative agreement (solid curves correspond to equation (15*b*)).

For the description of the $\varepsilon_5$ CEF line shift caused by an increase of the temperature the above mentioned electron–electron interaction mechanism (given in detail in [23]) is sufficient to explain the small shift of the $\varepsilon_5$ CEF level (line through □-symbols).

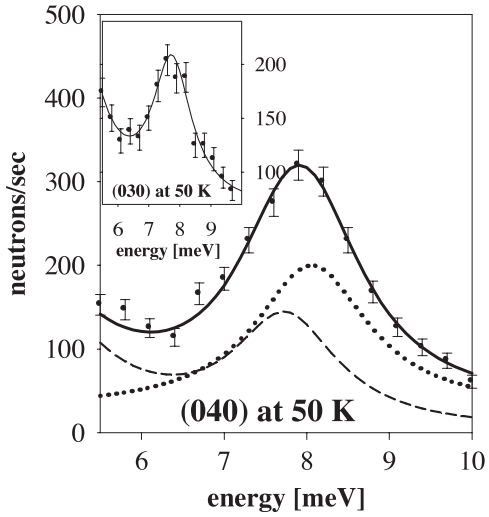


**Figure 8.** Neutron scattering intensity in the vicinity of the (040) Γ-point (•). The intensity is mainly caused by the phonon scattering mechanism, although a contribution due to the $\varepsilon_4$ CEF scattering will still exist at this high $\kappa$-value. The full curve through the data points is calculated taking into account both scattering mechanisms. The dotted and the dashed curves are the contributions of the 7.5 meV $A_g$-phonon mode and the $\varepsilon_4$ CEF level, respectively. Inset: neutron peak shape and position of the $\varepsilon_4$ CEF level at the (030) zone boundary (the curve is a guide for the eye).

### *6.3. Influence of the CEF–phonon interaction on the phonons*

For the investigation of the 7.5 meV $A_g$-phonon mode shift due to the CEF–phonon interaction, measurements at the (040) Γ-point were performed. Due to the much larger vector $\kappa$ (compared to the (020) Γ-point as before) the phonon scattering will dominate the neutron peak intensity.

In figure 8 an example is given. In the main frame the neutron scattering intensity measured at the (040) Γ-point is shown. The inset shows the neutron scattering intensity at the (030) zone boundary (both data are measured at 50 K). As can be seen from figure 2(a) the (030) peak shown in the inset depicts the $\varepsilon_4$ CEF level at the zone boundary. The dotted and the dashed curves are the positions of the 7.5 meV phonon mode and the $\varepsilon_4$ CEF level at 50 K, respectively. The full curve through the data points results from the combined effects of both scattering mechanisms. To determine the shift of the 7.5 meV $A_g$-phonon mode position in the scope of the theory given above the self energies $\Sigma_Q^1$ and $\Sigma_Q^2$ in equation (20) have to be calculated. For the theoretical CEF broadening we make use of the replacement $\eta^{0+} \rightarrow \Delta$ (analogous to the replacement given by equation (21)), and apply it in the equations (19*b*), (19*c*) for the phonon self energies. The numerical value for $\Delta$ (=0.9 meV) was obtained as an average of the FWHM of the neutron peaks in the range from 50 K to room temperature.

In figure 9 the neutron scattering intensity at the (040) Γ-point at various temperatures is given by the symbols. The line through the data points are (as explained for the 50 K data in figure 8) due to the dominating phonon scattering and those caused by the CEF contribution. The centre of gravity of the $A_g$-phonon mode peak has been determined and presented by ▼-symbols in figure 10. The full curve shows the calculated shift of the 7.5 meV $A_g$-phonon mode given by equation (20). As a further proof that the observed temperature shift of the 7.5 meV $A_g$-phonon mode in $NdCu_2$ is indeed due to the CEF–phonon interaction we have studied the temperature shift of the corresponding $A_g$-phonon mode of the isostructural nonmagnetic $YCu_2$ compound. Since there is no CEF–phonon interaction, any shift of phonon modes can

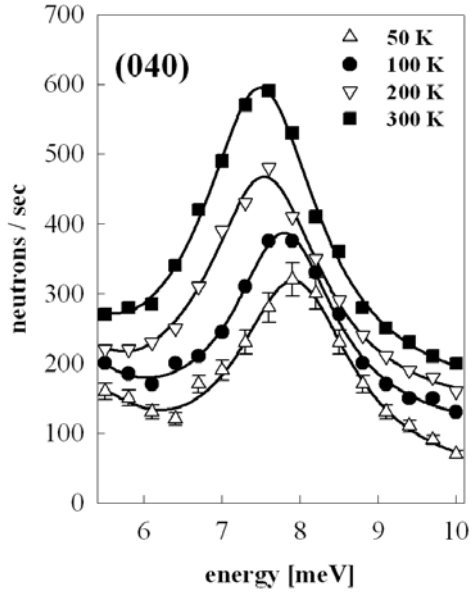


**Figure 9.** Temperature dependence of the 7.5 meV $A_g$-phonon mode measured at the (040) Γ-point. The lines through the data points are calculated taking into account both scattering mechanisms (as explained in connection with figure 8).

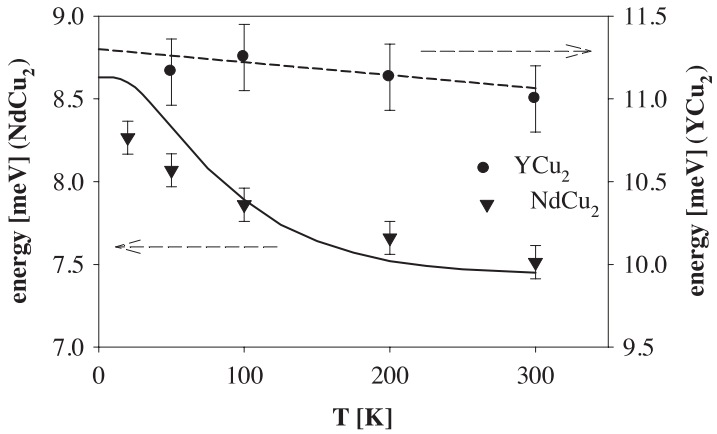


**Figure 10.** Temperature dependent shift of the 7.5 meV $A_g$-phonon mode of $NdCu_2$ together with the corresponding $A_g$-mode of $YCu_2$. The full curve gives the calculated $A_g$-phonon mode shift according to equation (20). The dashed line through the $YCu_2$-data points is due to the shift of the $YCu_2$ $A_g$-phonon mode caused by the electron–electron interaction mechanism.

only be caused by the electron–electron interaction. The lattice dynamics of this nonmagnetic compound has been presented in [19].

## 7. Conclusion

The most essential results of this work can be summarized as follows:

- The lattice dynamics of $NdCu_2$ has been studied by inelastic neutron diffraction experiments on a single crystal and on a powdered sample material (figures 2 and 3).
- The single crystal data were fitted by an axially symmetric Born–von Karman spring model. For a satisfying fit of the neutron data at least 10 springs with 20 force constants are required.

- A comparison of the calculated PDOS (from the Born–von Karman fit) and the measured PDOS (from a time-of-flight experiment) shows good agreement.
- We have confirmed a measurable CEF–phonon interaction in this orthorhombic intermetallic compound studying the interplay of the $\varepsilon_4$ CEF excitation and the 7.5 meV $A_g$-phonon mode as a function of temperature.

## Acknowledgments

We are grateful to W Reichardt (FZ Karlsruhe) and M Loewenhaupt (TU Dresden) for cooperation in part of the single crystal experiments and for very valuable discussions. The single crystal experiments were mainly carried out on the UNIDAS spectrometer at the FZ Juelich and in parts at the E1 spectrometer at HMI Berlin (supported by the European Community, contract number HPRI-CT-2001-00138, BENCS Nr.: PHY-02-0306, EU project number 183). We also wish to thank E Goremychkin for his support during the LRMECS experiment at IPNS Argonne National LAB.

## References

[1] Reichardt W and Nücker N 1984 *J. Phys. F: Met. Phys.* **14** L135
[2] Thalmeier P and Fulde P 1982 *Phys. Rev. Lett.* **49** 1588
[3] Thalmeier P 1984 *J. Phys. C: Solid State Phys.* **17** 4153
[4] Dörfer W and Schaack G 1985 *Z. Phys.* B **59** 283
[5] Ruf T, Heyen E T and Cardona M 1992 *Phys. Rev.* B **46** 11792
[6] Heyen E T, Wegerer R and Cardona M 1991 *Phys. Rev. Lett.* **67** 144
[7] Heyen E T, Wegerer R, Schoenherr E and Cardona M 1991 *Phys. Rev.* B **44** 10195
[8] Wegerer R, Thomsen C, Ruf T, Schoenherr E and Cardona M 1993 *Phys. Rev.* B **48** 6413
[9] Loewenhaupt M, Gratz E, Pillmayr N and Müller H 1990 *Physica* B **163** 427
[10] Loewenhaupt M, Prager M, Gratz E and Frick B 1988 *J. Magn. Magn. Mater.* **76/77** 415
[11] Gratz E, Loewenhaupt M, Divis M, Steiner W, Bauer E, Pillmayr N, Mueller H, Nowotny H and Frick B 1991 *J. Phys.: Condens. Matter* **3** 9297
[12] Takayanagi S, Amazaki H, Shibuya N, Sugawara Y, Svoboda P, Onuki Y, Settai R and Wada N 1995 *Physica* B **206/207** 395
[13] Svoboda P, Doerr M, Loewenhaupt M, Rotter M, Reif F, Bourdarot F and Burlet P 1999 *Europhys. Lett.* **48** 410
[14] Kramp S, Doerr M, Rotter M, Loewenhaupt M and Kamp R v d 2000 *Eur. Phys. J.* B **18** 559
[15] Sugiyama K, Settai R, Azuma H, Sugawara H, Aoki Y, Sato H, Kindo K and Onuki Y 1996 *Physica* B **216** 316
[16] Rotter M, Loewenhaupt M, Kramp S, Reif T, Pyka N M, Schmidt W and Kamp R v d 2000 *Europhys. J.* B **14** 29
[17] Kramp S, Loewenhaupt M and Rotter M 2000 *Physica* B **276–278** 628
[18] Nguyen H L, Franse J J M and Nguyen H H 2001 *J. Magn. Magn. Mater.* **224** 30
[19] Hense K, Gratz E, Lindbaum A, Michor H, Nowotny H, Güthoff F, Hoser A and Knoll P 2003 *J. Alloys Compounds* **349** 28
[20] Loewenhaupt M, Rotter M and Kramp S 2000 *Physica* B **276–278** 602
[21] Eyring H, Walter J E and Kimbell G E 1940 *Quantum Chemistry* (New York: Wiley)
[22] Walter U 1984 *J. Phys. Chem. Solids* **45** 401
[23] Fulde P and Loewenhaupt M 1986 *Adv. Phys.* **34** 589
[24] Hutchings M T 1964 *Point Charge Calculations of Energy Levels of Magnetic Ions in Crystalline Electric Fields* (*Solid State Physics* vol 16) ed F Seitz and D Thurnbull (New York: Academic)
[25] Taylor P L 1970 *A Quantum Approach to the Solid State* (Englewood Cliffs, NJ: Prentice-Hall)
[26] Herzfeld Ch M and Meijer P H 1961 *Group Theory and Crystal Field Theory* (*Solid State Physics* vol 12) ed F Seitz and D Thurnbull (New York: Academic)
[27] Hense K 1999 Gitterdynamik in der orthorhombischen Verbindung $YCu_2$ *Master Thesis* TU-Wien
[28] Mahan G F 1990 *Many-Particle Physics* 2nd edn (New York: Plenum)
[29] Hense K 2002 CEF–phonon interaction in the orthorhombic compound $NdCu_2$ *PhD Thesis* TU-Wien
[30] Lovsey S W 1984 *Theory of Neutron Scattering by Condensed Matter* vol 1 (Oxford: Science)